Science of the Total Environment 1020 (2026) 181542

Contents lists available at ScienceDirect

Science of the Total Environment

journal homepage: www.elsevier.com/locate/scitotenv

Organic carbon composition and preservation in macrotidal coastal wetland sediment: insights from biomarkers and isotopic signatures

Amann Benjamin [a,*], Dubillot Bénédicte [a], Eric Chaumillon [a], Cornelia Rumpel [b], Marie-France Dignac [b], Axel Felbacq [b], Sabine Schmidt [c], Maël Destampes [a], Marie Arnaud [b], Edouard Metzger [d], Thomas Lacoue-Labarthe [a], Christine Dupuy [a]

[a] LIttoral ENvironnement et Sociétés (LIENSs), UMR 7266 CNRS, La Rochelle Université, 17000, La Rochelle, France
[b] UMR 7618 CNRS, Sorbonne Université, INRAE, IRD, Institut of Ecology and Environmental Sciences (IEES), Paris, France
[c] Univ. Bordeaux, CNRS, Bordeaux INP, EPOC, UMR 5805, F-33600, Pessac, France
[d] Univ Angers, Nantes Université, Le Mans Université, CNRS, Laboratoire de Planétologie et Géosciences, LPG UMR 6112, 49000, Angers, France

HIGHLIGHTS

- Depth-resolved multimarkers reveal habitat-specific organic carbon preservation.
- Salt-marsh stores most organic carbon, but mudflats are also important.
- Mudflat organic matter degrades 3 times faster with depth than salt-marsh OM.
- Lignin is abundant in marshes, scarce yet persistent in mudflat sediments.
- OM decay slows below 5–10 cm, marking habitat-specific preservation depths.

GRAPHICAL ABSTRACT

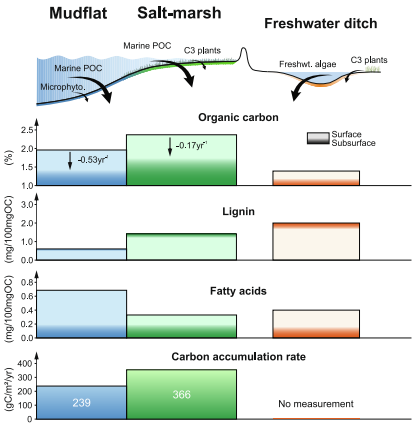

ARTICLE INFO

Keywords:
Blue carbon
Fatty acids
Lignin phenols
Stable carbon isotopes
Carbon accumulation rates
Salt-marsh and mudflat
Wave tide-dominated estuary

ABSTRACT

Coastal wetlands store high amounts of organic carbon (OC) in their sediments, but long-term preservation of this carbon depends on habitat type, sediment depth, and the molecular characteristics of organic matter (OM). This study explores the dynamics of OC deposition and preservation across vertical profiles (0–30 cm) in two adjacent coastal habitats—mudflat, and salt-marsh—within the macrotidal system of the Aiguillon Bay (France). A multi-tracer approach was applied, combining stable isotopes $\delta^{13}C$, C/N ratios, lignin phenols, and fatty acids. Sediment OC content ranged from 13.4 to 23.2 mgC g^{-1}, with the highest concentrations found in the salt-marsh. $\delta^{13}C$ and C/N signatures revealed dominant marine source in the mudflat, with a secondary contribution from microphytobenthos, and mixed marine–C_3 plant inputs in the salt-marsh. Fatty acids and lignin compositions supported this partitioning, with surface mudflat layers enriched in labile microbial and algal-derived compounds, whereas deeper salt-marsh sediments retained more resistant, C_3 plant-derived signatures resembling

* Corresponding author.
E-mail address: benjamin.amann.france@gmail.com (A. Benjamin).

https://doi.org/10.1016/j.scitotenv.2026.181542
Received 29 July 2025; Received in revised form 30 January 2026; Accepted 9 February 2026
Available online 20 February 2026

those of terrestrial OM source. OM degradation rates were closely linked to source composition and depth. Degradation was concentrated within the top 5 cm of salt-marsh and the top 10 cm of mudflat. Below these depths, biomarker profiles changed minimally, delineating a transition to longer-term preservation. First-order degradation constants were three times higher in mudflat (0.53 yr^{-1}) than in salt-marsh (0.17 yr^{-1}), despite similarly high sedimentation rates (1.8 and 2.2 cm yr^{-1}, respectively). This reflects differences in OM lability, with even minor contributions from microphytobenthos enhancing reactivity in mudflats. Salt-marshes, with their intermediate OM reactivity and high sedimentation rates, emerged as hotspots of carbon accumulation (366 gC m^{-2} yr^{-1}), while mudflats also contributed substantially to coastal carbon sequestration (239 gC m^{-2} yr^{-1}). These results highlight the value of depth-resolved, biomarker-based approaches to identify habitat-specific degradation dynamics; ultimately better understanding carbon accumulation in coastal ecosystems.

1. Introduction

Coastal wetlands—including salt-marshes, and intertidal mudflats—are increasingly recognized as effective carbon sinks, capable of storing organic carbon (OC) in sediments over decadal to millennial timescales (Alongi, 2020; Regnier et al., 2022). Their contribution to climate mitigation is now well documented, yet the long-term stability of OC in these environments is highly variable and site-dependent, depending on habitat characteristics (Windham-Myers et al., 2019). Carbon accumulation rates (CARs) in salt-marshes span several orders of magnitude; the most recent global CAR estimate averages 168 ± 7 gC m^{-2} yr^{-1} with values ranging from 1.2 to 1167.5 gC m^{-2} yr^{-1} (Wang et al., 2021). Similar variability has also been documented regionally in temperate French salt-marshes with CAR ranging from 75 to 345 gC m^{-2} yr^{-1} (Amann et al., 2024). CARs in tidal mudflats also vary substantially, with a global mean CAR of 130 ± 30 gC m^{-2} yr^{-1} and values ranging from 2 to 1129 gC m^{-2} yr^{-1} (Chen and Lee, 2022). Understanding the factors that control OC preservation after burial is essential for accurately assessing the sequestration potential of these systems.

Carbon storage in coastal wetlands is influenced by multiple interrelated factors, including the origin and chemical properties of organic matter (OM), sedimentation rates, microbial activity, and redox conditions specific to each environment (Macreadie et al., 2025). Organic matter inputs in coastal wetlands can derive from marine and terrestrial sources and vary in composition according to the dominant vegetation, litter type and hydrological setting, which strongly influence OM degradability after burial (Arnaud et al., 2024; Leorri et al., 2018; Van de Broek et al., 2018). Once deposited, OM is subjected to depth-dependent diagenetic processes such as oxidation (Bradley et al., 2022), bioturbation (Aller and Cochran, 2019) and microbial degradation (Qiao et al., 2018). These processes are influenced by local conditions in oxygen levels, sediment compaction, and sediment composition influencing organo-mineral associations (Macreadie et al., 2025; Windham-Myers et al., 2019). As a result, OM stabilization may occur at varying depths across wetland types, yet the mechanisms and thresholds involved are not fully understood.

To assess carbon preservation, depth-resolved characterizations of OM quantity and quality are required. Classical approaches, such as loss-on-ignition (LOI) and elemental analysis (CHN), remain widely applied for estimating OC content (Wang et al., 2021). Their combination with stable isotope analysis ($\delta^{13}C$) allows insight into OM sources – such as marine vs terrestrial sources – and compositional shifts distinguishing between contributions from C_3 and C_4 plants, and has been implemented across various coastal settings (Lamb et al., 2006). Yet, similar isotopic signatures among intertidal halophytes and terrestrial litter can complicate the attribution of OM sources.

To overcome these limitations, several studies have turned to complementary biomarkers. Lignin phenols, resistant molecules specific to vascular plant tissues, have been used to trace terrestrial inputs and assess OC degradation status through ratios such as syringyl/vanillyl (S/V), cinnamyl/vanillyl (C/V), and acid-to-aldehyde (Ad/Al) indices (Bianchi and Canuel, 2011; Goñi and Hedges, 1992). These markers have proven especially useful in differentiating between woody/herbaceous and gymnosperm/angiosperm inputs and in detecting microbial or fungal alterations (Liang et al., 2023). Vaughn et al. (2020), for example, used a combination of stable isotopes, CHN, and lignin phenols to show high inputs of woody material in the mangrove-transition salt-marsh zones along the southern U.S. coast, with implications for OC degradation rates. Lipid-based biomarkers such as fatty acids provide additional insight into both the origin and diagenetic state of sedimentary OM, due to their structural diversity and sensitivity to microbial processing (Bianchi and Canuel, 2011). Specific fatty acid signatures have been used to identify microbial inputs and assess OM degradation states (Middelburg and Herman, 2007; Qiao et al., 2018). Long-chain fatty acids, phytosterols, and 18:3ω3 markers have been used to trace halophyte-derived organic matter from salt-marshes to adjacent tidal flats of Mont Saint Michel Bay (Meziane et al., 1997). Combined elemental and biomarker approaches—including C/N ratios, $\delta^{13}C$, and lignin phenols—have been applied to characterize terrigenous OC inputs in marine sediments in the Golf of Mexico (Goñi et al., 1998), and to track OM sources and degradation state in shelf and estuarine systems in China (Xia et al., 2021). Strategies integrating multiple OM markers such as $\delta^{13}C$, $\delta^{15}N$, lipids, and lignin parameters have also been used to reconstruct OM dynamics along land–sea continuums and in permafrost-influenced coastal systems (Lin et al., 2025). Together, these studies demonstrate the advantages of a multi-tracer approach for a more comprehensive understanding of OC sources and preservation dynamics in coastal wetland sediments. Nevertheless, comprehensive depth-resolved applications of such combined tracers across distinct wetland habitats remain rare. Also, while many blue carbon studies focus on long-term carbon accumulation over decadal to centennial timescales, few examine the early phase of organic carbon deposition and preservation. Understanding these initial dynamics is critical, as they set the foundation for long-term sequestration potential, even though they do not directly represent multi-decadal carbon stocks.

In this context, this study investigates the composition, origin, and degradation state of OC along vertical sediment profiles in two adjacent coastal wetland habitats – a mudflat, and a salt-marsh – located in the Aiguillon Bay, Southwestern France. A combination of bulk geochemical indicators (OC, C/N, $\delta^{13}C$) and compound-specific biomarkers (lignin phenols and fatty acids) is used to assess the variability of OM sources and reactivity with depth. By identifying depth-dependent degradation patterns together with ^{210}Pb-based sediment accumulation rates, the analyses aim to refine the current understanding of the early phase of organic carbon deposition and decadal-scale carbon preservation across contrasting coastal wetland environments.

2. Study area

To investigate sedimentary carbon deposition and preservation dynamics, two adjacent coastal habitats – a mudflat (MD) and a salt marsh (SM) – were selected from the Aiguillon Bay in southwestern France. Aiguillon Bay forms a shallow coastal embayment that opens into the Pertuis Breton, a flooded incised valley between Ré Island and the Vendée coast (Weber et al., 2004). The bay is partially enclosed by the Pointe de l'Aiguillon to the northwest, a sandy spit extending obliquely across its mouth. The region is subject to a semidiurnal macrotidal regime, with tidal ranges reaching up to 6.5 m during spring tides (Dodet et al., 2019),

and features extensive intertidal flats and salt-marsh systems. Rapid sediment-infilling within the Poitevin Marsh, followed by centuries of land reclamation and wetland management have led to fast coastal progradation (Baumann et al., 2017; Chaumillon et al., 2004). Today, the bay comprises 3700 ha of mudflats and 1100 ha of salt-marshes.

Sediment and freshwater inputs to the Pertuis Charentais are primarily supplied by the Sèvre Niortaise River (mean discharge: 12 $m^3 s^{-1}$; Banque HYDRO, 1969–2017), with additional contributions from a network of artificial channels including the Curé and Canal de Villedoux to the south, and the Chenal Vieux and Canal de Luçon to the north (Fig. 1b). These fluvial sources result in persistently high suspended sediment concentrations in the shallow waters of the Pertuis Charentais, maintained throughout the year by the sheltering effect of Oléron and Ré islands (annual mean coastal suspended particulate matter >40 g m^{-3}; Amann et al., 2024). Wind waves and tidal currents further enhance mud resuspension, sustaining elevated suspended sediment levels in the area (Bassoullet et al., 2000).

The mudflat is primarily colonized by biofilms of microphytobenthos, especially benthic diatoms, which contribute significantly to the primary production (Blanchard et al., 2002). The salt-marsh exhibits typical tidal zonation along the intertidal gradient: *Halimione portulacoides* (sea purslane) dominates the mid-marsh (up to 25% cover), *Spartina maritima/anglica* occurs mainly in lower marsh (1–2% cover), and *Agropyron* species are found in in the upper marsh (27–30% cover; data LIFE Aiguillon, 2022). Over the last three decades—corresponding to the time interval covered by the sediment cores—the coring sites have remained within the same habitat types (upper mudflat and lower salt-marsh dominated by *Halimione p.*, respectively). Although salt-marsh progradation has occurred at the scale of the bay, local conditions at the sampling sites remained stable (Amann et al., 2023).

A third site – a backshore freshwater ditch (FD) – was also included to assess the contribution of terrestrial organic matter from the Poitevin Marsh to carbon inputs in the Aiguillon Bay (Fig. 1). This freshwater ditch is embedded within a network of anthropogenically modified channels, which drain cultivated cereal fields and grasslands established on former retro-littoral marshlands (Fig. 1b). While backshore canals are regularly dredged to maintain water levels, this selected freshwater ditch had remained undisturbed since 2016–2018. This provides a snapshot of the sedimentary organic matter pool that could be mobilized during dredging, representing a sediment source end-member. Although beyond the reach of tidal influence, these low-lying zones maintain lateral exchanges of water and sediment with the coastal bay through riverine outflow.

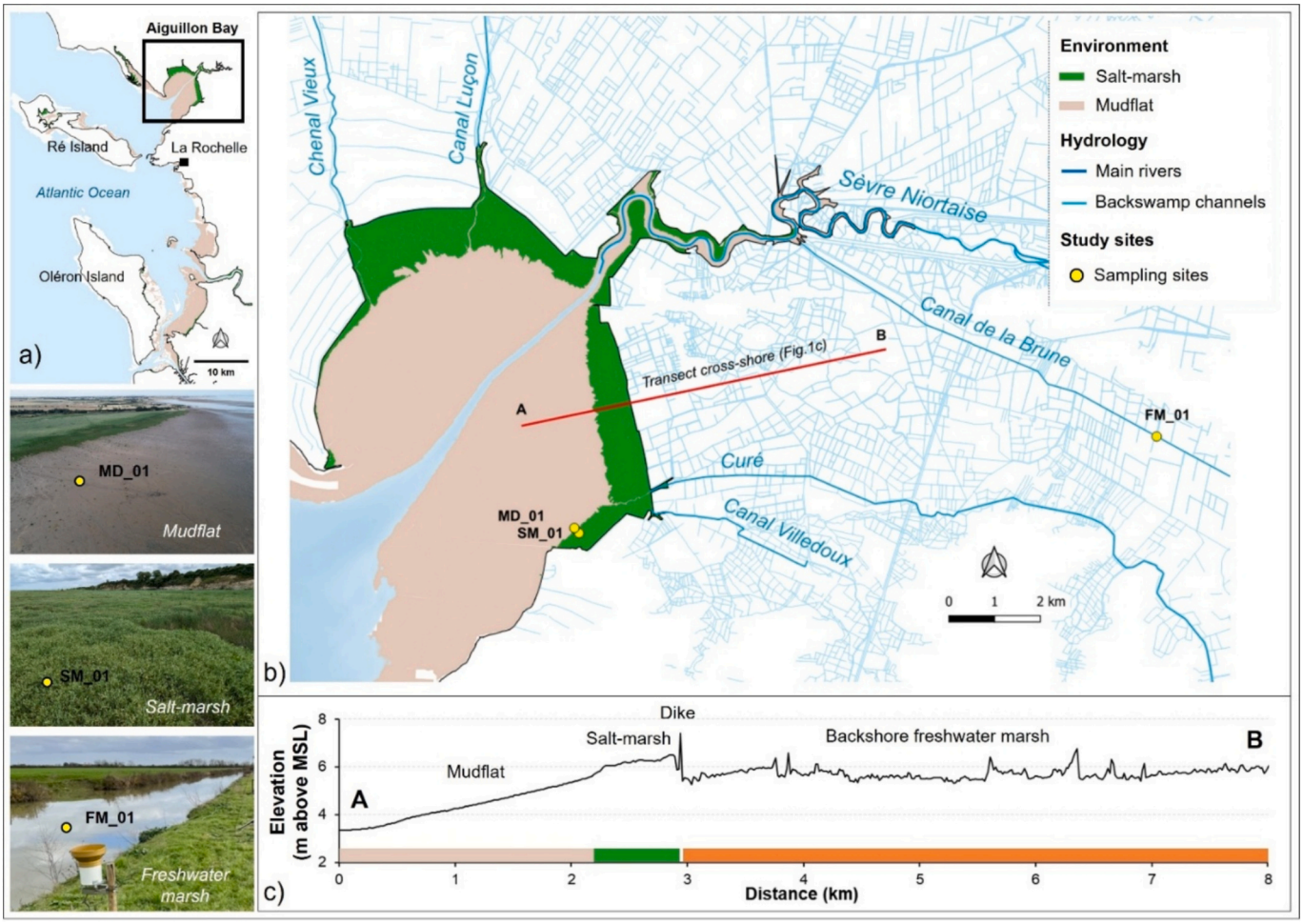

Fig. 1. a) Location of the study area along the French Atlantic coast, north of La Rochelle and near Ré Island. b) Close-up of Aiguillon Bay with key coastal habitats: intertidal mudflats, salt-marshes, and the backshore freshwater environment connected by a dense network of backswamp channels. Sampling locations are marked with yellow dots: mudflat (MD_01), salt-marsh (SM_01), and freshwater ditch (FM_01). c) Topographic transect from sea to land, illustrating habitat distribution and elevation gradient across the study site (in m above mean sea level MSL).

3. Materials and methods

3.1. Sample collection and conditioning

Sediment sampling was conducted in April 2023 from the lower salt-marsh (SM 01) and the adjacent upper mudflat (MD 01; Fig. 1). At each site, three replicate cores were collected to a depth of 30 cm using an 87 mm-diameter corer (UWITEC, Austria). Repeated sampling at the same location aimed to minimize operational errors and to ensure replication in environment where microtopography, sediment composition, plants and biofilm distribution may be spatially heterogeneous (e.g., Douglas et al., 2024). Cores were extracted during low tide in the upper mudflat zone, and in the *Halimione portulacoides* belt of the salt-marsh, which corresponds to the dominant and only perennial species (Amann et al., 2023). Sediment cores were also collected from the freshwater ditch site to assess the sediment organic matter composition of typical dredged backshore canals that might differ from fluvial sources. The core depth was selected based on previous studies in the Aiguillon Bay salt-marsh (Amann et al., 2024), which showed that most changes in OC content occur in the upper 20–30 cm. Sampling was further optimized to ensure sufficient material for multiple biomarker analyses (e.g. lignin, fatty acids, stable isotopes), which are time-consuming and –for some analyses– material-intensive. In the laboratory, cores were sectioned into depth intervals of 0–1, 1–5, 5–10, 10–20, and 20–30 cm. Samples were frozen at −20 °C immediately after slicing, then freeze-dried and homogenized using a ceramic mortar.

To assess sediment accumulation and organic carbon burial rates in coastal habitats, complementary 1-m long sediment cores were collected in 2022 from the mudflat and salt-marsh using a peat auger (Eijkelkamp, Netherlands). These cores were dedicated specifically to radionuclide dating and mass flux estimates. The peat auger's pivoting blade limited compaction, offering reliable depth profiles for sedimentation rate analysis. However, its semi-open design was less suited for biomarker preservation, as exposure to air during sampling could degrade labile compounds such as lignin and lipids. This dual-coring approach allowed for high-resolution geochemical characterization while securing independent estimates of sedimentation rates in the mudflat and salt-marsh settings. Because active ditch maintenance (e.g., dredging) can compromise sediment stratigraphic continuity, sediment accumulation and carbon burial rates were not assessed for the freshwater ditch site. This station was primarily used as a source indicator.

Primary producer material was collected on April 2023 near the coring sites to characterize organic carbon sources. In the salt-marsh and on the banks of the freshwater ditch, leaves and roots of dominant plant species were harvested, rinsed with distilled water, and stored frozen prior to freeze-drying. Microphytobenthos was recovered from the mudflat by scraping surface biofilms and allowing the samples to settle in light conditions through a 200 μm mesh, concentrating benthic microalgae. Finally, suspended sediment was collected by filtering water samples through pre-combusted 0.7 μm GF/F filters, then drying at 50 °C prior to analysis of suspended particulate organic carbon (POC).

3.2. Sediment, mass, and carbon accumulation rates

Sediment and mass accumulation rates (SAR in cm yr^{-1} and MAR in g cm^{-2} yr^{-1}) were estimated in the two coastal sites using excess ^{210}Pb ($^{210}Pb_{xs}$) profiles following the constant flux and constant sedimentation (CF:CS) model (Fig. S1; Data access: Schmidt and Amann, 2024). ^{210}Pb, a naturally occurring radioisotope with a half-life of 22.2 years, accumulates in sediments through atmospheric deposition. Excess ^{210}Pb ($^{210}Pb_{xs}$) decreases with depth according to its half-live and sedimentation rates. Activities of ^{210}Pb, ^{226}Ra, ^{137}Cs and ^{232}Th were measured using a Broad-Energy germanium detector, and $^{210}Pbxs$ was calculated by subtracting ^{226}Ra-supported activity from total ^{210}Pb. To account for variations in sediment properties (vegetation fraction, grain size), $^{210}Pb_{xs}$ values were normalized to ^{232}Th (referred to as $^{210}Pb_{xs}^{Th}$; Amann et al., 2024, 2023). Sedimentation and mass accumulation rates were further validated using ^{137}Cs ($T^{1/2}$ = 30 years), an artificial isotope introduced by atmospheric nuclear weapon tests with a fallout peak in 1963 (Delaune et al., 1978).

Carbon accumulation rates or carbon burial rates (CAR in gC m^{-2} yr^{-1}) were calculated below surface active layers as the product of OC content (%) and sediment mass accumulation rate (MAR in g cm^{-2} yr^{-1}) derived from $^{210}Pb_{xs}^{Th}$ profiles. The extent of this surface layer was determined through depth-profile analysis of degradation markers, such as labile fatty acids.

3.3. Elemental and stable isotope analyses

Organic carbon (OC) content and stable carbon isotope ratios ($\delta^{13}C$) were analyzed on decarbonated sediment samples, suspended sediment samples, and plant material collected from each site. A second round of analysis was performed from each sample prior to decarbonation to determine nitrogen content (N), thus allowing estimates for organic carbon to nitrogen ratios (OC:N, hereafter referred as C/N). Analyses were performed using an elemental analyzer (EA Isolink, Thermo Scientific) coupled to a continuous-flow isotope ratio mass spectrometer (Delta V Plus with Conflo IV interface, Thermo Scientific; analytical precision <0.10‰) at the LIENSs Stable Isotope Facility, La Rochelle University. $\delta^{13}C$ values are expressed in delta notation (‰) relative to the Vienna Pee Dee Belemnite (VPDB) standard using the formula:

$$\delta^{13}C = \left[R\_sample / R\_standard - 1 \right] \times 1000; \text{where R is the ratio of } {}^{13}C/{}^{12}C.$$

Isotopic and elemental data ($\delta^{13}C$, and C/N ratios) were used to evaluate the origin of sedimentary organic carbon along the land–sea continuum.

Source attribution was based on primary producers and suspended particulate organic carbon sampled directly in this study. These included microphytobenthos from the mudflat, dominant salt-marsh plants (e.g., *Halimione, Agropyron, Puccinellia and Spartina*), and plant species characteristics of the freshwater ditch surroundings (e.g., *Carex, Salix, Galium, Sinapis*). Suspended POC was also collected from both coastal and freshwater environments to represent aquatic sources. These end-members provided a representative baseline for evaluating the origin and transformation of organic matter across sediment cores.

3.4. Source mixing model

Two-end-member mixing models were used to visualize and quantify source contributions from $\delta^{13}C$ vs C/N biplots for each habitat. The choice of binary models was motivated by the fact that sedimentary values aligned along clear binary mixing $\delta^{13}C$ – C/N spaces, suggesting two main sources of sedimentary OC distinct across habitat. For mudflat samples, marine POC and microphytobenthos were considered as end-members; for salt-marsh samples, marine POC and C_3 halophytic vegetation; and for freshwater marsh samples, freshwater algae and C_3 freshwater plants. Source contributions were estimated by projecting sediment sample coordinates onto the line defined by the two end-members, as:

$$f_1 = \frac{(X_{sample} - X_2)(X_1 - X_2) + (Y_{sample} - Y_2)(Y_1 - Y_2)}{(X_1 - X_2)^2 + (Y_1 - Y_2)^2} \quad ; \quad f_2 = 1 - f_1$$

where $f1$ and $f2$ are the fraction of end-member 1 and 2 respectively, X and Y represent C/N and $\delta^{13}C$, and subscripts 1 and 2 refer to end-members 1 and 2, respectively. These binary models were used to provide illustrative, first-order estimates of dominant source contributions and to support discussion of OM lability across habitats. However, they were interpreted with caution, as other potential sources and diagenetic processes may influence sediment signatures.

3.5. Lignin-phenol extraction and analysis

Lignin-derived phenols were extracted using alkaline copper oxide (CuO) oxidation, following the protocol of Hedges and Ertel (1982) and modified by Kögel and Bochter (1985). Prior to lignin extraction, plant roots were cryogenically ground using liquid nitrogen and a ball mill to obtain a fine, homogeneous powder. Aboveground plant tissues and sediment samples were dried, finely ground, and processed without cryogenic treatment.

500 mg of dry sediment or 70 mg of dry-plants materials were oxidized in sealed Teflon-lined reactors with a reagent mixture of 250 mg CuO, 50 mg ammonium iron (II)-sulfate hexahydrate, 50 mg glucose, and 2 M NaOH at 172 °C under nitrogen (N_2) for 2.5 h. Post-oxidation, ethylvanillin was added as an external standard to evaluate product recovery. The oxidation mixture was acidified to pH 1.8–2.2 with 6 N HCl, brought to constant volume, and left for 75 min in the dark to allow humic acids to precipitate. Lignin oxidation products were then extracted on C18 solid-phase columns (Macherey-Nagel), derivatized with *N*, *O*-Bis(trimethylsilyl)trifluoroacetamide (BSTFA), and analyzed using gas chromatography (GC 6890, Agilent) equipped with a SGE BPX-5 column (60-m length, 0.25-mm inner diameter, 0.32-Am coating) and a flame ionization detector. GC settings followed a multistep oven temperature ramp from 100 °C to 300 °C. One microliter of each sample was injected in split mode (1:10), with helium as the carrier gas. Phenylacetic acid was used as an internal standard for quantification.

CuO oxidation yields characteristic phenolic compounds grouped into vanillyl (V), syringyl (S), and cinnamyl (C) units. Lignin content (Λ) is reported as the sum of these three phenol groups, normalized to 100 mg of organic carbon. The acid-to-aldehyde ratio of syringyl units $(Ad/Al)_s$ was used as a diagenetic indicator, reflecting the oxidative degradation state of lignin (Bianchi et al., 2009; Dodla et al., 2012). The ratios C/V and S/V were used to discuss OM sources and degradation, the cinnamyl and syringyl components degrading faster than vanillin (Opsahl and Benner, 1995).

3.6. Fatty acid extraction and analysis

Ester-linked fatty acids (FAs) were determined with the ester-linked fatty acid methyl ester method (EL-FAME) to characterize the community composition of living microorganisms (Li et al., 2020). Fatty acids were extracted from 3 g of freeze-dried samples and methylated at 37 °C using 15 mL of 0.2 M KOH/MeOH solution for 1 h, followed by a neutralization through 3 mL of 1.0 M of acetic acid. Fatty acid methyl ester extraction was done with 3 mL of hexane and total evaporation under N_2 flow. Dried EL-FAMEs were then resuspended in 500 μL of hexane, of which 180 μL was transferred to a vial with 20 μL of 19:0 internal standard (methyl nonadecanoate acid). The analysis of EL-FAMEs was performed with an Agilent 6890 N gas chromatograph equipped with a flame ionization detector and a SGE BPX70 column (60 m, 0.32 mm, 0.25 μm). Ultra-high purity helium was used as a carrier gas. The column was kept at 80 °C for 1 min and then heated to 160 °C at a rate of 25 °C/min, to 180 °C at a rate of 2 °C/min and finally heated to 220 °C at a rate of 3 °C/min and kept at 220 °C for 10 min. The injector was kept at 280 °C and the detector at 350 °C. A volume of 1 μL was injected at a split ratio 1:10. Peaks were identified using FAME mix and Bacterial FA mix standards (Supelco). Fatty acid concentrations were normalized to 100 mg of organic carbon.

3.7. Kinetics of OM degradation

To assess the degradation dynamics of sedimentary OC, a first-order kinetic model was applied to sediment profiles of mudflat and salt-marsh. For this, the 1-D Single-G model originally proposed by Berner (1980) and adapted by Middelburg (1989) was used to estimate apparent degradation rate constants (k, in yr^{-1}) in both mudflat and salt-marsh sediments. The model could not be applied to the backshore freshwater marsh as active ditch maintenance (e.g., dredging) restrained sediment accumulation rate estimates. The Single-G model follows a parabolic decay trend expressed as:

$$OC(t) = a.e^{-kt} + b$$

where OC(t) is the organic carbon content (%), t is sediment age estimated from sediment accumulation rates (yr), a is the size of the reactive OC pool, k is the apparent degradation rate constant (yr^{-1}), and b represents the residual refractory OC fraction. Model fitting was performed using non-linear least squares regression (nls) in R. The goodness-of-fit was evaluated using the coefficient of determination (R^2) and Shapiro–Wilk normality test on the residuals (*p-value*).

This 1-D Single-G approach considers that OC reactivity gradually decreases over time, without dividing it into specific compound types or categories. While more complex models involving discrete reactivity classes may better capture the mechanistic heterogeneity of organic matter pools (Stolpovsky et al., 2018), the Single-G model allows for simple comparison between OC degradation patterns across sediment types. Degradation rate constants were calculated assuming constant sediment accumulation through time, as supported by the linear fit of excess ^{210}Pb activity under the CF:CS model and consistent sedimentation rates across the full core depth. The estimated apparent degradation rate k was then compared to the three OC reactivity classes proposed by Stolpovsky et al. (2018): Highly active OC ($k \approx 70\ yr^{-1}$), active OC ($k \approx 0.5\ yr^{-1}$), and refractory OC ($k \approx 0.001\ yr^{-1}$).

3.8. Statistical analysis

Differences among habitats were assessed using the non-parametric Kruskal–Wallis test for each parameter, followed by Dunn's post-hoc test when the null hypothesis was rejected. Differences between surface and deeper sediment layers within each coastal habitat were evaluated using the Wilcoxon signed-rank test, with the 0–5 cm interval considered as surface and 10–30 cm as depth (Hollander et al., 2013). Non-parametric tests were selected to account for the relatively limited number of data points, despite the use of three replicates per core.

A principal component analysis (PCA) was performed to explore multivariate relationships among all measured variables across the two coastal habitats. The quality of variable representation was evaluated using squared cosine (cos^2) values. Spearman's rank correlation was also used to examine pairwise associations between variables. All statistical analyses were conducted using R software (R Core Team 2023, version 4.3.3; R packages: rstatix – Kassambara A, 2023: https://rpkgs.datanovia.com/rstatix/; ggfortify - Horikoshi and Tang, 2018: https://CRAN.R-project.org/package=ggfortify).

4. Results

4.1. Sediment and mass accumulation rates

Sediment from both the mudflat and salt-marsh environments exhibit high sediment accumulation rates, with excess $^{210}Pb_{xs}$ detected at depth greater than 100 cm, indicating prolonged rapid sedimentation over several decades (Fig. S1). Detrital inputs, as indicated by ^{232}Th activities (30–50 mBq g^{-1}), were slightly lower in the upper sections of the cores, likely reflecting dilution by organic-rich material. Dry bulk density (DBD) profiles were relatively homogeneous (~1.0 g cm^{-3}), with limited compaction with depth, suggesting stable sediment accumulation and minimal textural variation.

Sediment accumulation rates (SAR) estimated from the $^{210}Pb_{xs}^{Th}$ profiles reached 2.2 ± 0.4 cm yr^{-1} in the salt-marsh and 1.8 ± 0.1 cm yr^{-1} in the mudflat. The respective mass accumulation rates (MAR) were 2.1 ± 0.3 g cm^{-2} yr^{-1} for the salt-marsh and 1.7 ± 0.1 g cm^{-2} yr^{-1} for the mudflat. ^{137}Cs was detected throughout the profiles but the length of the cores was insufficient to capture the 1963 fallout peak. Given the

high accumulation rates, the 1963 ^{137}Cs fallout peak was indeed calculated to lie below the base of the 1-m cores at c. 133 cm in the salt marsh and c. 110 cm in the mudflat. The slight increase in ^{137}Cs activity observed toward the base of the cores supported these high accumulation rates (Fig. S1).

4.2. Organic carbon content and sources

OC content differed between habitats, with OC significantly decreasing with depth ($p < 0.015$) in the two coastal sites (Fig. 2). The highest mean OC was observed in the salt-marsh, decreasing from 23.2 $\pm$ 2.2 mg g^{-1} at the surface to 17.6 $\pm$ 0.4 mg g^{-1} at 30-cm depth. In the mudflat, values dropped from 19.8 $\pm$ 0.1 mg g^{-1} to 13.4 $\pm$ 0.2 mg g^{-1} between surface and deeper layers.

The δ^{13}C and C/N signatures of dominant organic matter sources—including halophyte plants, microphytobenthos, plant litter, and the sediment signature of the freshwater ditch—are shown in Fig. 3. These end-member signatures were used as reference points to interpret the composition of sedimentary organic matter across habitats. The dominant halophytic plant species such as *Halimione, Agropyron, and Puccinellia* reflected typical C_3 plant signatures (C/N ratio from 12 to 20; δ^{13}C ~ −28‰), while *Spartina* exhibited a distinct C_4 plant δ^{13}C signature around −14‰ and a relatively high C/N ratio (12.5). The freshwater plant species *Galium, Sinapis*, Salix and *Carex* presented a typical C3 signature. Microphytobenthos collected from the mudflat had δ^{13}C values (−15.2‰) and a C/N ratio (7.7) consistent with marine algal sources.

δ^{13}C values significantly differed among habitats ($p = 3.18e^{-9}$), while C/N ratios were statistically similar between salt-marsh and freshwater ditch sediments ($p = 0.7$). In the mudflat, δ^{13}C and C/N values generally matched those of coastal marine suspended particulate organic carbon (POC). However, a slight enrichment in ^{12}C was observed with depth ($p < 0.01$), but no significant depth-related trend in C/N ($p = 0.13$). In the salt-marsh, sediment δ^{13}C and C/N signatures fell between those of coastal marine POC and C_3 plant inputs, but more closely resembled the marine end-member. Sediment organic matter from the freshwater ditch showed a mixed signal reflecting both freshwater POC through high algal input and local C_3 freshwater vegetation. Following the application of two-end-member mixing models, the mudflat OC composition suggested a mean contribution of 91% marine POC and 9% microphytobenthos. In contrast, the salt-marsh OC composition reflected 87% marine POC and 13% vascular C_3 plants. The sediment composition of the freshwater ditch aligned along a freshwater mixing trajectory suggesting 87% algal and 13% C_3 plant-derived OC, which does not appear to influence sediment composition of the coastal sites (Fig. 3).

4.3. OC degradation rates

Degradation rate modeling using the Single-G model revealed distinct OC decay patterns between mudflat and salt-marsh sediments (Table 1; Fig. 4). In the mudflat, OC content declined rapidly with depth and time, following a steeper decay curve and exhibiting a higher apparent degradation rate constant (k = 0.53 yr^{-1}, R^2 = 0.92). In contrast, the salt-marsh sediments showed a slower decline in OC content, with a lower degradation rate constant (k = 0.17 yr^{-1}, R^2 = 0.71).

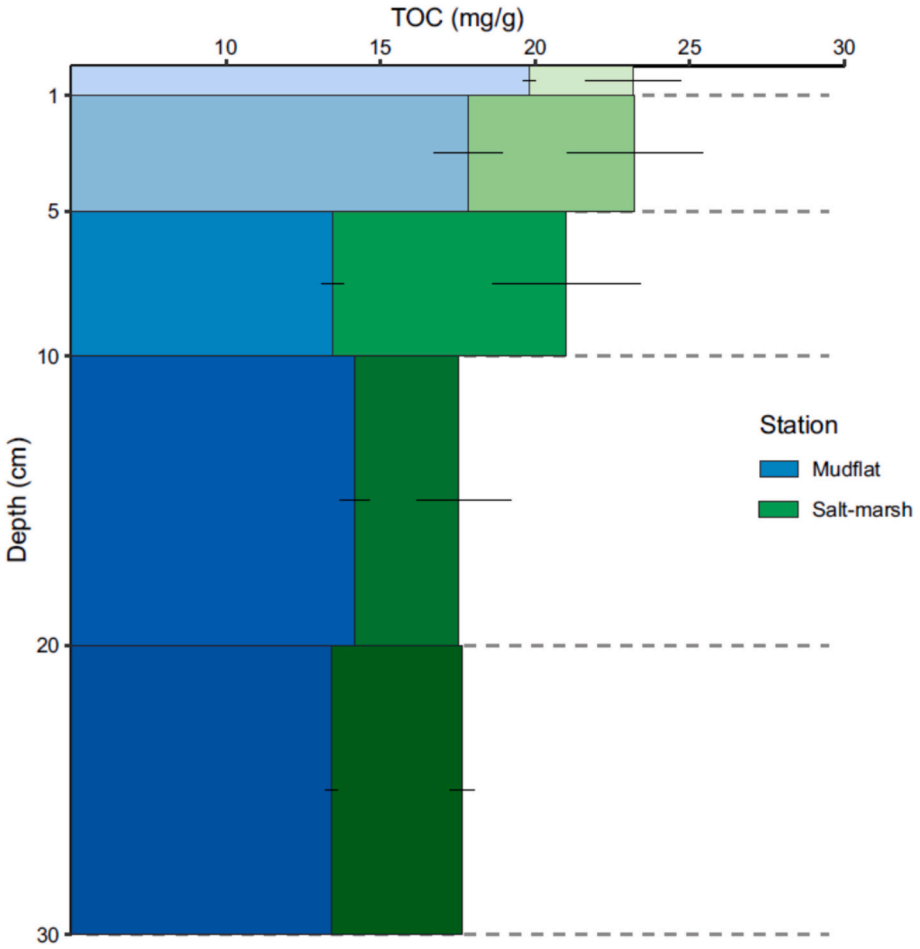

Fig. 2. a) Sediment profiles of organic carbon content (OC, in mg g^{-1}) for the salt-marsh and mudflat. Mean OC values and standard deviation ($n = 3$) are positioned at sediment mid-depth. Note that the superimposed histogram highlights the higher OC content observed in the salt-marsh sediments.

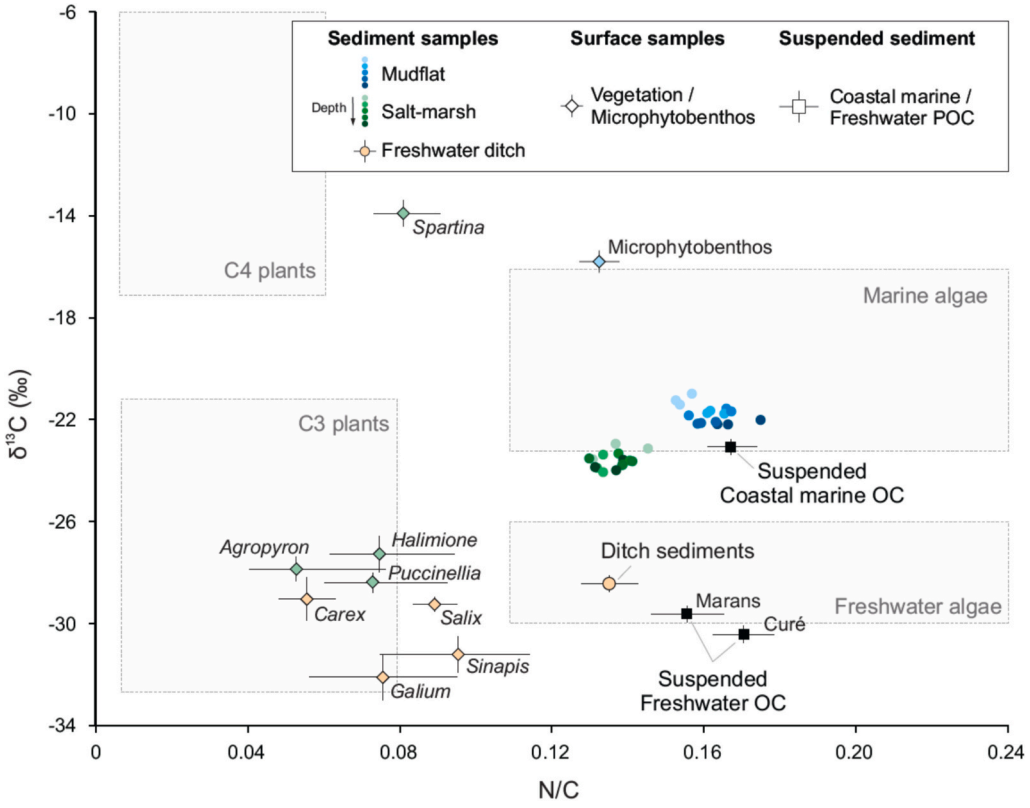

Fig. 3. Comparison of $\delta^{13}C$ (‰ ± SD) and N/C signatures of sediment samples at different depths (0–30 cm) and for the two coastal habitats: salt-marsh (*green circles*) and mudflat (*blue circles*). Source material: freshwater ditch sediments (orange circle), coastal marine and freshwater POC from suspended sediment (*black squares*); and surface samples (*diamonds*) for different groups of plants (halophytic: *green diamonds;* freshwater: *orange diamonds*), and microphytobenthos (*diamonds*). Data from this study are compared with the signature of C_3- and C_4-plant, and with marine and freshwater algae signature from the literature (*gray areas*; Alongi, 2020 and Lamb et al., 2006, respectively). The use of N/C as *x* axis allows better separating the OM sources, graphically.

Table 1
Rate constant of degradation *k* (in yr^{-1}) for salt-marsh and mudflat sediments, modeled using the first-order single G-model (Berner, 1980) through asymptotic OC decrease with depth.

Station	Model Equation	Rate constant k	R^2	Residual Normality (Shapiro-Wilk)	Notes
Mudflat	$OC = a{\cdot}e^{-kt+b}$	0.53 yr^{-1}	0.92	$p = 0.94$	Strong fit
Salt marsh	$OC = a{\cdot}e^{-kt+b}$	0.17 yr^{-1}	0.71	$p = 0.80$	Good fit

Both models fit the observed data well, with normally distributed residuals ($p > 0.05$, Shapiro–Wilk test), supporting the suitability of the Single-G approach. Because sediment accumulation rates were constant over the dated interval, vertical OC trends reflected post-depositional degradation rather than changes in initial OC inputs.

4.4. Lignin-phenol biomarkers

Lignin concentrations (mg/100 mg OC) varied significantly among environments (Fig. 5). The lowest values were found in mudflat sediments (0.4 ± 0.09 mg/100 mg OC), while significantly higher

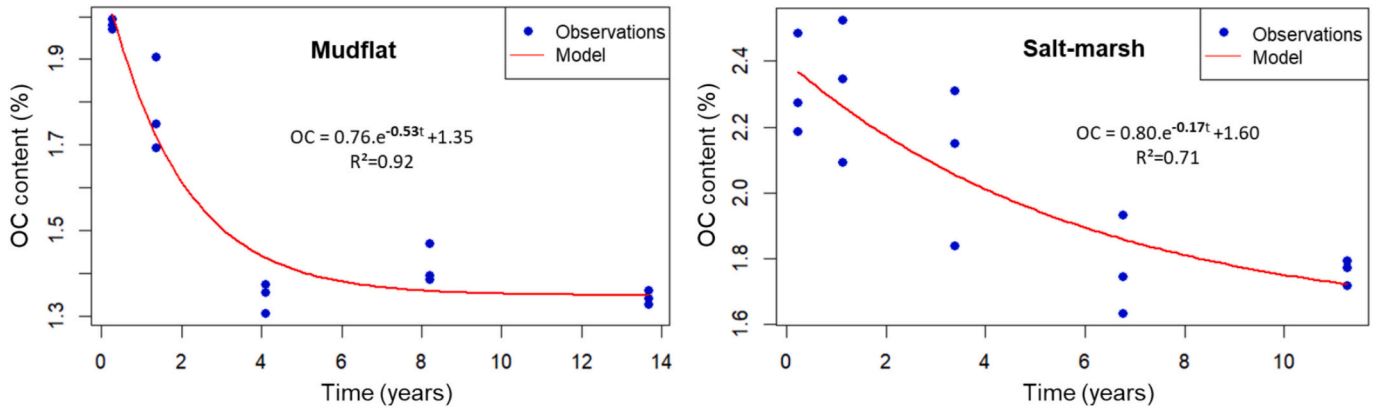

Fig. 4. Temporal evolution of the organic carbon content (OC, in %) fitted with a single exponential decay model (Single-G model, Berner 1964) in surface sediments of mudflat (*left*) and salt-marsh (*right*). Blue dots represent observed OC values over time (t, years), and red lines represent the model fit using the following equation: $OC = a.e^{-kt} + b$.

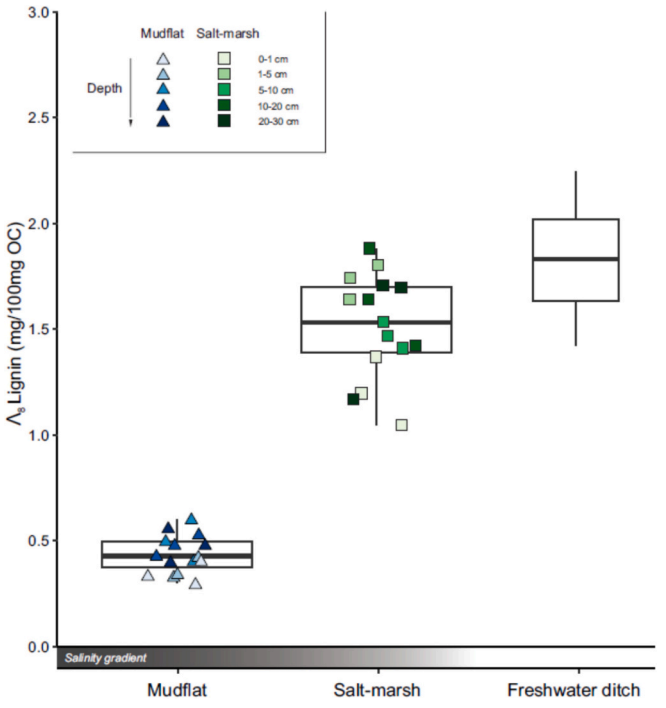

Fig. 5. Boxplot illustrating the distribution of normalized lignin content (Λ_8) in sediment at different depths for the mudflat (MD), and salt-marsh (SM) sites, compared to the mean sediment signature of the freshwater ditch site. All points with three replicates per depth are presented for the coastal sites. No significant variation with depth was detected.

concentrations were observed in salt-marsh sediments (1.5 ± 0.3 mg/100 mg OC; $p < 0.001$), similar to those found in the freshwater ditch site (1.8 ± 0.3 mg/100 mg OC; $p > 0.05$).

Syringyl-to-vanillyl (S/V) and cinnamyl-to-vanillyl (C/V) ratios ranged from 1.0 to 2.3 and 0.1–0.2, respectively, for all samples (Fig. 6). These values indicated a predominant input from angiosperm vegetation, though there were clear compositional differences among habitats. Salt-marsh sediments showed the highest S/V ratios (mean 1.7 ± 0.4), which significantly differ from mudflat (1.3 ± 0.2) and freshwater ditch sediments (1.2 ± 0.1; $p < 0.01$). Mudflat sediments exhibited slightly higher C/V ratios (0.14 ± 0.054) than both the salt-marsh (0.11 ± 0.04) and the freshwater sites (0.09 ± 0.02). The lignin signatures observed in salt-marsh sediments (high S/V and low C/V ratios) were similar to those found in the roots of *Halimione portulacoides* (S/V = 2.80, C/V = 0.09), the dominant species in this habitat. In contrast, the roots of *Spartina maritima*, present at the mudflat edge, exhibited lower S/V (1.3) and higher C/V (0.5) ratios, consistent with the composition of the adjacent mudflat sediments (Fig. 6; Fig. S1).

The acid-to-aldehyde ratio of syringyl units ((Ad/Al)s) also varied among habitats (Fig. 7). Mudflat sediments displayed significantly higher (Ad/Al)s values (0.24 ± 0.03) than those from the salt-marsh (0.15 ± 0.02; $p < 0.001$), which resembled those of the freshwater ditch (0.17 ± 0.01). No significant differences in (Ad/Al)s with sediment depth were observed in the coastal habitats ($p > 0.05$).

4.5. Fatty acids

Total fatty acid (TFA) concentrations varied significantly ($p < 0.05$) among habitats (Fig. 8a; Table S1), with higher levels in the mudflat (0.38 ± 0.16 mg/100 mg OC) than in the salt-marshe (0.24 ± 0.11 mg/100 mg OC) and the freshwater ditch (0.27 ± 0.08 mg/100 mg OC). TFA concentrations in sediments of both the mudflat and the salt-marsh declined significantly with depth ($p < 0.01$). Sediments were primarily composed of short-chain (SCFAs), monounsaturated (MUFAs), and bacterial fatty acids (BAFAs), all of which decreased with depth ($p < 0.01$), except BAFAs in the salt-marsh, which remained stable ($p = 0.7$). Long-chain (LCFAs) and polyunsaturated fatty acids (PUFAs) were less abundant and showed no consistent depth-related variation (Fig. 8b).

Surface mudflat sediments were relatively rich in SCFAs and BAFAs compared to the salt-marsh ($p < 0.01$). BAFAs comprised 25% of surface FAs in the mudflat, and only 13% in the salt-marsh. Deeper layers showed more comparable BAFA proportions across habitats ($p > 0.05$). Fatty acid profiles did not change significantly below 5 cm in the salt-marsh and 10 cm in the mudflat. Below these depths — which correspond to the first 3 to 6 years of sedimentation, respectively — total FA levels in both the mudflat and the salt marsh did not differ statistically.

Across all samples, the ubiquitous C16:0 was the most abundant fatty acid (20–30% of total FAs), followed by habitat-specific markers such as C16:1ω7 (notably in the mudflat and the freshwater ditch) and C18:1ω9 (more prevalent in the salt-marsh and the freshwater ditch). The mudflat was further distinguished by its high surface concentrations of C14:0 and C15:0 (Table S1).

4.6. Synthetic view of biomarkers: a multivariate analysis

The PCA provides an overview of various variables: TOC, C/N ratio, $\delta^{13}C$, lignin and fatty acids in sediment characteristics of the two coastal habitats (Fig. 9). These variables were well separated into two principal dimensions, accounting for 74.8% of the total variation (axis 1: 43.2%, axis 2: 31.6%). The first dimension was largely driven by the acid-to-aldehyde ratio of syringyl units (Ad/Al)s, lignin content, and the C/N ratio and $\delta^{13}C$ signature. The second dimension was primarily explained by fatty acid biomarkers (BAFA, SCFA, PUFA, MUFA), which were strongly positively correlated. TOC and the S/V ratio were well represented by both dimension 1 and dimension 2, likely due to high values found in surface sediment samples of the salt marsh. LCFA was correlated to TOC but showed poor representation in the PCA ($cos^2 < 0.2$).. The C/V ratio was correlated with (Ad/Al)s, but was also poorly represented in the PCA biplot ($cos^2 < 0.1$).

The signatures of coastal sediments at different depths (0–30 cm) were also plotted and differentiated well in these two principal dimensions. In the mudflat, the surface sediments were positively correlated with fatty acids along dimension 2, while the deeper sediment was positively correlated with (Ad/Al)s and $\delta^{13}C$ along dimension 1, showing a gradient with depth. In the salt-marsh, surface sediment was positively correlated with TOC, lignin, and C/N ratio along dimension 1, while the deepest salt-marsh sediment samples were not well projected to dimensions 1. Salt marsh samples followed a surface-to-depth gradient toward decreasing TOC and fatty acids, with a less depleted $\delta^{13}C$ signature (Fig. 9a). The distribution of sedimentary data along this PCA space was interpreted through two pathways (Fig. 9b) with: (i) an OM source pathway separating marine OC from terrestrial OC, for which the mudflat samples clearly differed from the salt marsh samples, and (ii) an OM degradation pathway associated to systematic depth gradient across habitats, distinguishing an OC- and TFA-richer sediment surface.

5. Discussion

5.1. Organic carbon sources across habitats

The origin of sedimentary OC differed significantly among the studied habitats, shaped by contrasting primary production regimes and hydrodynamic connectivity. $\delta^{13}C$ and C/N pointed to clear binary mixing spaces with dominant marine contributions in both mudflat (91%) and salt-marsh sediments (87%), with microphytobenthos as a key additional source in the mudflat (9%) and C3 halophytic vegetation in the salt-marsh (13%). In this context, the source of the freshwater sediment appeared to have a minimal influence on the $\delta^{13}C$ and C/N signatures of the coastal sediment OM. Whether in suspension in the tributaries or accumulated in the freshwater ditch, sediments showed

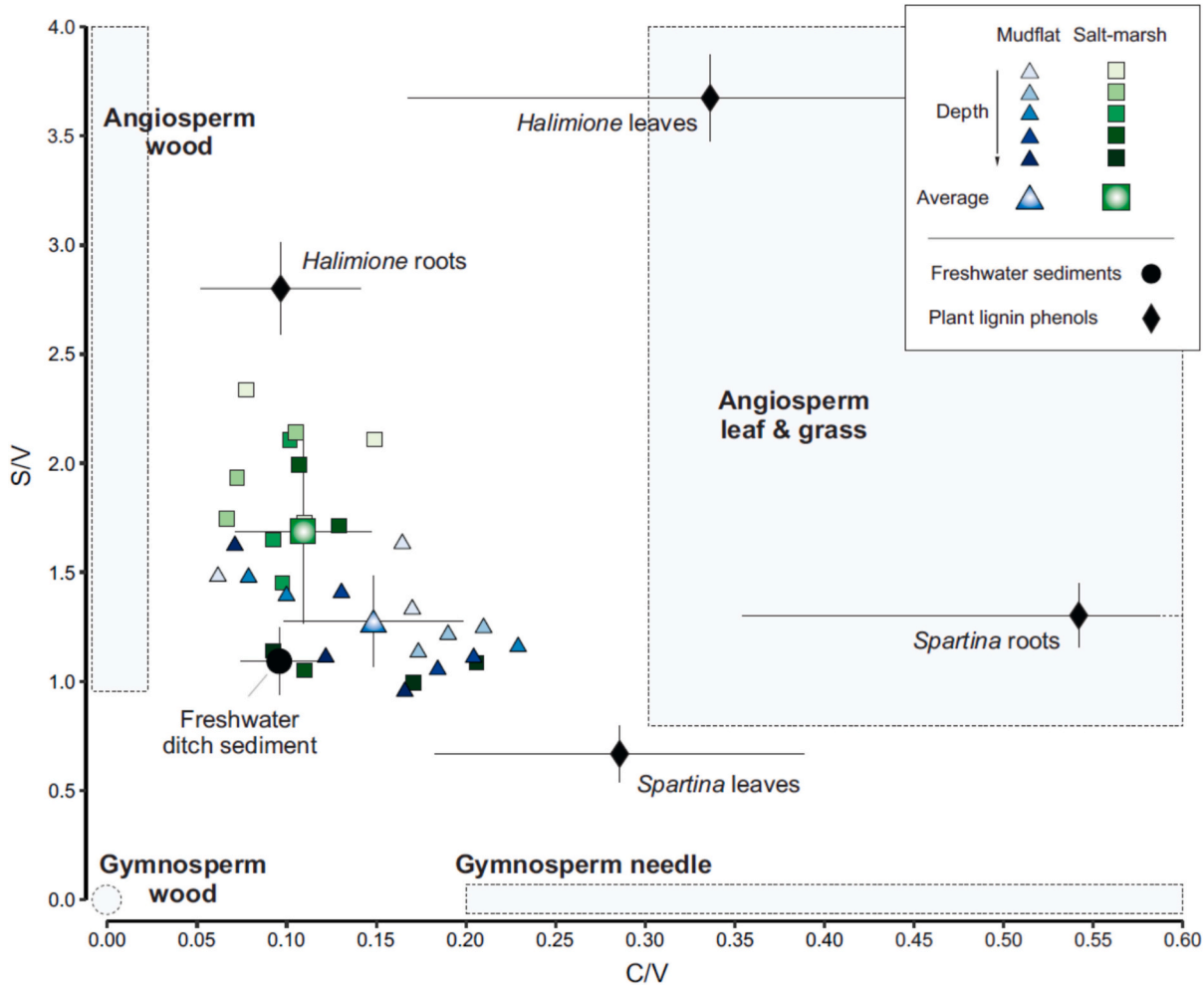

Fig. 6. Scatter plots of the weight ratios of Syringyl to Vanillyl phenols (S/V) versus Cinnamyl to Vanillyl phenols (C/V) of sediment with depth from the mudflat, and the salt-marsh, compared to the mean sediment signature of the freshwater ditch site. S/V and C/V for plants (leaves and roots) representative of coastal habitats from Aiguillon Bay are also illustrated: *Halimione portulacides* and *Spartina maritima*. The mean values and standard deviations for each habitat are represented by crosses and error bars, respectively. All points with three replicates per depth are presented and compared with the literature ranges for woody and non-woody tissues of both angiosperm and gymnosperm vegetation (gray areas) (Goñi and Hedges, 1992).

more depleted $\delta^{13}C$ values and relatively higher C/N ratios. This sediment signature dominated by freshwater algal (c. 85%) and C_3 plant-derived OC (c. 15%) is consistent with the reported phytoplanktonic activity and seasonal blooms in ditch sites (Moncelon et al., 2022), and is in line with studies on riverine-to-estuarine gradients (Bouillon and Boschker, 2006; Van de Broek et al., 2018; Lamb et al., 2006; Leorri et al., 2018). While the binary models provide first-order estimates of the dominant source contributions, they should be considered indicative rather than definitive due to potential overlap in source signatures and transformations during early diagenesis. Other biomarkers are used in this study to discuss organic sources in more details. Yet, the dominance of marine POC as the primary OC source in the sediment of coastal habitats aligns with the macrotidal and minerogenic nature of the Aiguillon Bay. Strong tidal currents and low river discharge (c. 12 m^3 s^{-1}) facilitate the deposition of sediment and POC (Middelburg and Herman, 2007). This mechanism is illustrated by the high sediment accumulation rates (c. 2 cm yr^{-1}) in the Aiguillon Bay, which are among the highest reported worldwide (Amann et al., 2024; Chen and Lee, 2022).

Total lignin and phenols, exclusively derived from vascular plant tissues, provided further insight into source attribution. Lignin concentrations were the lowest in the mudflat (c. 0.5 mg/100 mg OC), reflecting low terrestrial OC inputs and the dominance of marine-derived material (Ladd et al., 2019). In contrast salt-marsh and freshwater ditch sediments contained a markedly higher lignin content (c. 1.5 mg/100 mg OC), which is consistent with enhanced contributions from local vegetation and litterfall (Wang et al., 2021; Xia et al., 2021). Salt-marsh sediments exhibited slightly higher S/V ratios indicative of halophytic plant inputs such as *Halimione*. In contrast, the higher C/V and (Ad/Al)S ratios in mudflat sediments pointed to inputs from herbaceous monocot halophytes like *Spartina* pioneer species that locally colonize the upper mudflat zone and/or herbaceous fluvially-transported litter with limited preservation (Goñi et al., 1993).

Fatty acid (FA) profiles, although accounting for less than 0.7% of OC, supported the inferred source partitioning across habitats. Mudflat surface layers were enriched in labile FAs, particularly SCFAs, PUFAs and BAFAs, commonly associated with diatoms and microbial sources (Dai et al., 2009). A similar, though less pronounced, pattern was observed in the freshwater ditch site, where surface FAs primarily reflected inputs from freshwater algae (Table S1). In contrast, salt-marsh sediments exhibited lower total FA content, approximately half that of the mudflat, which is consistent with higher inputs of more recalcitrant vascular plant material.

Together, the results revealed a clear gradient of OC sources, from marine-dominated mudflats enriched in microbial OM, to salt-marsh sediments containing a mixture of marine and vascular plant inputs,

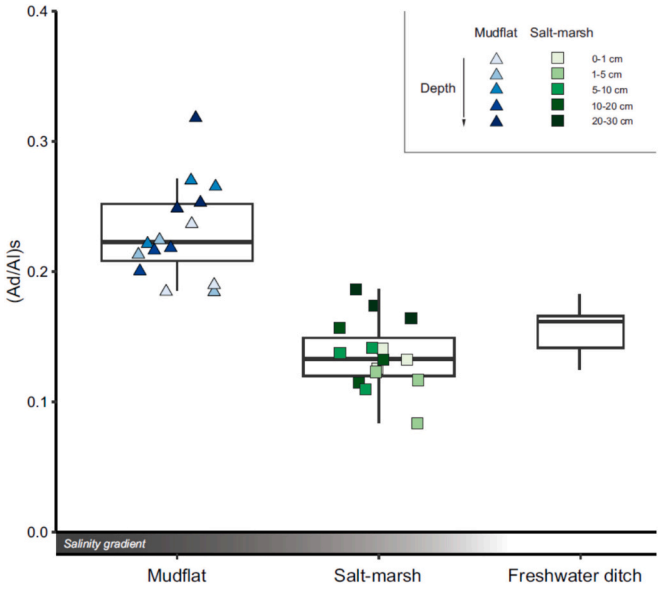

Fig. 7. Boxplot of the Acid/Aldehyde ratio of syringyl units (Ad/Al)s from the salt marsh and mudflat at different sediment depths (0–30 cm), compared to the mean sediment signature of the freshwater ditch site. All points with three replicates per depth are presented.

and freshwater ditch sediments dominated by algal and terrestrial sources. The $\delta^{13}C$ and C/N values followed the expected estuarine patterns (Savoye et al., 2012; Van de Broek et al., 2018; Xia et al., 2021); however, their relatively high $\delta^{13}C$ values and low C/N ratios reflected limited terrestrial inputs. This pattern can be explained by the specific setting of Aiguillon Bay, as it is connected to a macrotidal, mixed tide- and wave-dominated estuarine system characterized by low river discharge and predominantly supplied with sediment from the sea.

In such environments, OM is extensively reworked by tidal resuspension and microbial activity (Savelli et al., 2019), as also observed in other macrotidal estuaries (Middelburg and Herman, 2007), leading to homogenized isotopic signatures. Biomarker data from the Aiguillon Bay thus provide a novel perspective on the composition and transformation of OM in low-discharge macrotidal estuaries, where tidal and wave energy, rather than river input, predominantly governs sedimentary OC dynamics.

5.2. Organic matter quality and preservation with depth

OM degradation rates across coastal habitats were closely linked to the identity and molecular characteristics of the source. Apparent degradation constants (k) from OC depth profiles fitted by a single-G model revealed a decay rate that was three times faster in the mudflat ($k = 0.53\ yr^{-1}$) than in the salt-marsh ($k = 0.17\ yr^{-1}$). These values fall within the range of 'active' organic matter as defined by Stolpovsky et al. (2018), who classified degradation rates as highly active ($70\ yr^{-1}$), active ($50\ yr^{-1}$) or refractory ($0.001\ yr^{-1}$); the mudflat thus aligns with the active fraction and the salt-marsh exhibits intermediate lability between the active and refractory pools.

In the mudflat, labile OM inputs from microphytobenthos and marine phytoplankton likely fuel rapid microbial degradation, as evidenced by the sharp surface decline of SCFAs, MUFAs (e.g., C16:1ω7), and BAFAs)—compounds known for their high lability (Dai et al., 2009). The steeper gradient of fatty acids and OC with depth supports an efficient early-stage mineralization, with concentrations relatively unchanged below c. 10 cm depth. This rapid decay in surface is consistent with the lower molecular weight and higher degradability of algal-derived OC, as well as the low lignin content of mudflat sediments (Bianchi et al., 2009). Slightly higher (Ad/Al)s in mudflat sediments suggest a more advanced lignin degradation stage compared to the salt-marsh, possibly due to pre-depositional oxidation during transport in oxygenated conditions (Goñi et al., 1998). However, given the relatively low (Ad/Al)s values, the influence of lignin source variability cannot be ruled out, as plant origin may also affect Ad/Al indices (Goñi et al., 2003, 1993).

In contrast, salt-marsh sediments, composed primarily of marine POC with contributions from C_3 halophytic vegetation, exhibited more moderate OC degradation with depth. This slower decay is consistent with a higher proportion of structurally resistant material, reflected in lower FA lability and elevated lignin content. Lower $(Ad/Al)_s$ ratios and moderate k values suggested lower OM degradation. This could be explained by a mixture of labile and more refractory OM that could

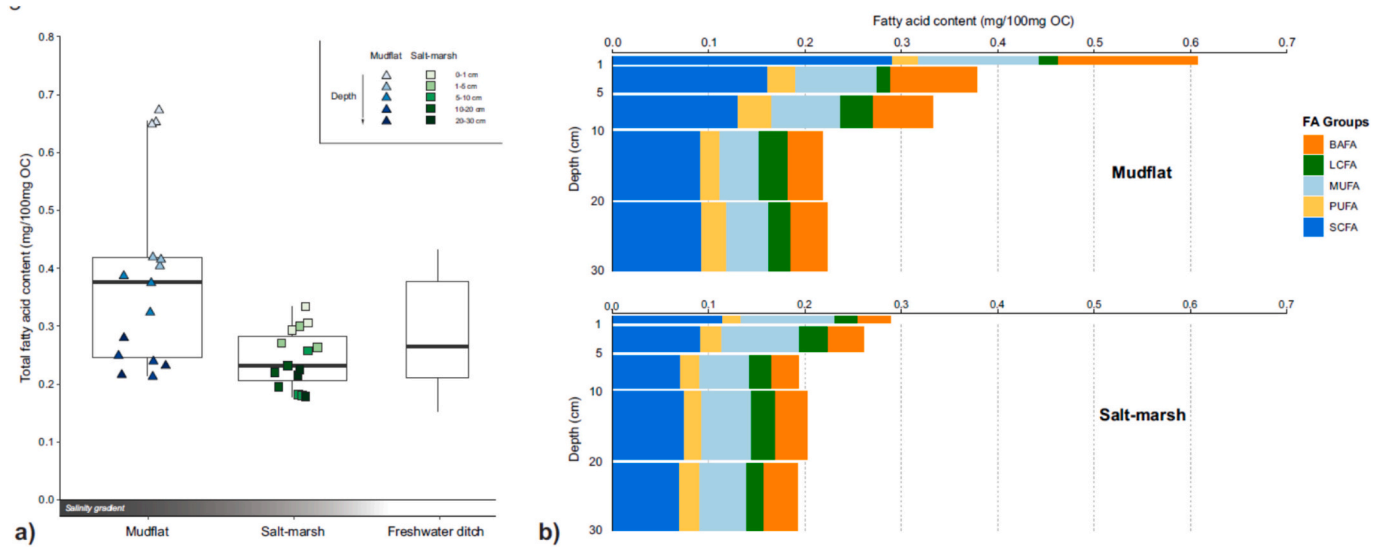

Fig. 8. a) Boxplot illustrating the distribution of normalized Total ester-linked Fatty Acid (TFA) measured with sediment depth in the two coastal sites, compared to the mean sediment signature of the freshwater ditch site. All points with three replicates per depth are presented. b) Depth profiles of normalized Fatty Acid biomarker content in the mudflat and the salt-marsh. FA grouping was based on literature with: SCFA, short-chain satured fatty acids (C8:0 to C21:0 without C15:0) (Cranwell, 1982); LCFA, long-chain satured fatty acids (C22:0 to C24:0) (Cranwell, 1982; Dai et al., 2005; Meziane et al., 1997); MUFA, monounsatured fatty acids; PUFA, polyunsatured fatty acids; BAFA, bacterial fatty acids (C15:0; C17:0; i-C15:0; ai-C15:0; i-C17:0) (Jeffries, 1972; Taylor and Parkes, 1983; Volkman et al., 1989).

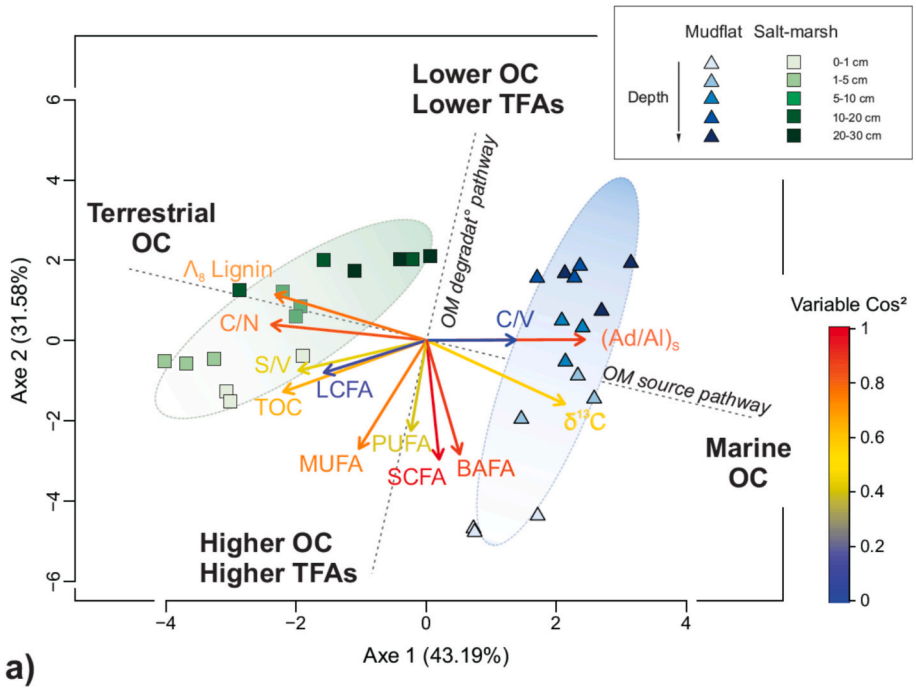

Fig. 9. a) Principal component analysis (PCA) performed on sediment samples from the mudflat (*blue triangles*), and the salt-marsh (*green squares*) in Aiguillon Bay. Symbols are color-coded by sediment depth (0–30 cm). Axes represent the first two principal components, explaining 41.1% and 31.6% of the total variance, respectively (cumulative: 72.7%). Variables include total organic carbon (TOC), $\delta^{13}C$, C/N ratio, total lignin (Λ), lignin-derived indices ($(Ad/Al)_s$, S/V, C/V), and fatty acid groups (SCFA, MUFA, PUFA, BAFA, LCFA). The color gradient of each arrow indicates the quality of its representation (cos^2) on the PCA plane, from blue (low) to red (high). Schematic interpretation of PCA sample distribution is also included through: an OM source gradient from marine to terrestrial material and a degradation gradient from surface to deeper layers.

reduce microbial activity (Dai et al., 2009). The input of mineral sediments in coastal wetlands may also protect organic carbon from decomposition by forming organic carbon-mineral complexes that are resistant to microbial attack (Macreadie et al., 2025). While mudflat samples followed a distinct mixing line between marine POC and microphytobenthos, salt-marsh points aligned more closely along a marine–C_3 plant axis (Fig. 3). Additionally, the sedimentary composition deviated from the OM degradation pathway at depth (Fig. 8). This subtle difference, with even a small contribution from microphytobenthos (c. 9%) in the mudflat, likely enhances OM lability explaining the faster degradation in the mudflat compared to the salt-marsh.

The persistence of lignin and long-chain fatty acids at depth further confirms the presence of resistant organic matter, consistent with patterns reported in other estuarine wetlands. Below habitat-specific surface-active layers—c. 5 cm in the salt-marsh and c. 10 cm in the mudflat—OC composition changed minimally, suggesting reduced microbial processing and enhanced preservation. This is also reflected in the decay of OC content reaching asymptotic levels. These patterns of mixed depth are well known in marine soft sediments (e.g., Teal et al., 2008), and the influence of active layers on carbon burial estimates is increasingly acknowledged for salt-marshes, albeit with site-specific variations (Amann et al., 2024; Van de Broek et al., 2018). However, this topic remains rarely addressed in mudflat systems (James et al., 2024). These findings demonstrate that the OM source and the diagenetic environment are important in shaping carbon preservation across coastal wetland sediments on the decadal scale.

5.3. Outwelling of organic matter across habitats

The compositional mismatch between salt-marsh and mudflat lignin signatures provided direct evidence that little marsh-derived particulate OM is deposited onto the mudflat surface. Despite their proximity, the mudflat did not record the molecular fingerprint of salt-marsh vegetation. This suggests weak lateral transfer of particulate OC between the two habitats, thus moderating the applicability of the outwelling hypothesis in the Aiguillon Bay. While Odum (1980) proposed that salt-marshes export substantial OM to adjacent coastal waters, subsequent works have shown that export is strongly system-specific and mediated by tidal energy, hydrodynamics, and marsh geomorphology (Childers et al., 2002; Santos et al., 2021).

In Aiguillon Bay, the salt-marsh platform is topographically higher and is inundated only ~5% of the time (present day conditions; Amann et al., 2024), whereas the upper mudflat is flooded during nearly every tide. Combined with dense halophytic vegetation that enhances the trapping of suspended sediments, these conditions favor net import from the mudflat to the marsh rather than export in the reverse direction. Such limited opportunity for marsh-to-mudflat transport, together with strong macrotidal resuspension, likely restricts the deposition of marsh-derived particulate OC onto the mudflat in the Aiguillon Bay. The relative ecological maturity of the Aiguillon Bay salt-marshes may further constrain particulate OC export, as older marshes generally exhibit lower net export due to near-equilibrium between production and respiration (Childers et al., 2002). In this context, the salt-marsh in Aiguillon Bay may function more like a system that retains and transforms organic matter internally, than as a significant source of particulate organic carbon to adjacent mudflats.

Although these conclusions are based on sediment core analyses rather than direct flux measurements, they align with observations from other macrotidal systems showing constrained outwelling under high-energy conditions (Santos et al., 2021). Future studies involving time-resolved monitoring of particulate and dissolved OC would better capture carbon flux dynamics and refine assessments of OM export in macrotidal systems. Specific attention could also be given to inorganic carbon—both particulate and dissolved—, as it can contribute significantly to tidal marsh export, thus influencing coastal carbon budgets and

its long-term buffering capacity of the coastal ecosystem (Wang et al., 2016).

5.4. Implications for carbon sequestration and habitat connectivity

Carbon burial rates (CAR) varied significantly across habitats, reflecting contrasts in hydrodynamic conditions, OM input and sediment retention capacity. CAR below active layers reached 366 gC m^{-2} yr^{-1} in the salt-marsh and 239 gC m^{-2} yr^{-1} in the mudflat. These rates exceeded both regional (231 ± 108 gC m^{-2} yr^{-1}; Amann et al., 2024) and global averages for salt-marshes (168 ± 7 gC m^{-2} yr^{-1}; Wang et al., 2021) and tidal flats (130 ± 30 gC m^{-2} yr^{-1}; Chen and Lee, 2022), placing the Aiguillon Bay among the highest documented coastal carbon sinks. These elevated rates are consistent with the macrotidal regime of Aiguillon Bay (spring tides up to 6.5 m), where strong tidal currents, a large tidal prism, and high suspended-sediment concentrations promote rapid sediment import and vertical accretion. CAR values of 239–366 gC m^{-2} yr^{-1} fall within the upper ranges reported for sediment-rich macrotidal systems, where salt marshes typically reach 250–400 gC m^{-2} yr^{-1} and tidal flats 150–300 gC m^{-2} yr^{-1} (Chen and Lee, 2022; Ouyang and Lee, 2014; Van de Broek et al., 2018). Nevertheless, these rates should be interpreted with caution, as they rely on single representative cores and may not fully capture spatial variability. The mudflat estimate likely represents the upper bound of tidal-flat burial, while the salt-marsh value lies at the high end of locally reported rates, consistent with enhanced sediment accumulation near the mudflat–marsh transition (Amann et al., 2023, 2024).

The combined dataset revealed that the potential for carbon sequestration in coastal wetlands depends not only on OC supply but on the interplay between source composition, degradation intensity, and sediment retention. Salt-marshes, with intermediate OM lability and high sedimentation rates (2.2 cm yr^{-1}), acted as hotspots of decadal-scale OC burial. Despite receiving more labile marine inputs, mudflats also supported substantial carbon burial due to rapid deposition (1.8 cm yr^{-1}), highlighting their under-recognized role in blue-carbon budgets (Chen and Lee, 2022; James et al., 2024; Macreadie et al., 2019). The progressive shift toward increasing marine signature with depth in salt-marsh sediments (PCA, Fig. 8) further suggests that long-term OC composition is shaped by tide- and wave-driven transport and preserved through mineral-organic interactions.

By integrating molecular biomarkers with sediment profiles in a macrotidal, low-fluvial-input environment, this study revealed mechanisms of OC accumulation often overlooked in blue carbon frameworks. While microtidal and mesotidal systems with high riverine discharge typically exhibit a substantial terrestrial OC supply and extensive estuarine processing (e.g., Ni et al., 2025; Xia et al., 2021), the patterns observed in Aiguillon Bay align with other macrotidal settings where marine-derived OM dominates (Meziane et al., 1997; Van de Broek et al., 2018). In this sediment-rich and hydrodynamically system, both vegetated and unvegetated habitats contributed meaningfully to carbon storage.

Together, these results emphasize that OC preservation in coastal wetlands is not solely governed by emergent vegetation cover but is strongly modulated by hydrodynamics, sediment connectivity, and habitat-specific degradation dynamics that shape lateral transport, trapping and burial of organic carbon. This perspective contrasts with deltaic and microtidal estuaries (Childers et al., 2002; Wang et al., 2021), and points to the need for site-specific, process-based approaches when assessing coastal carbon budgets. Extending this depth-resolved, biomarker-based framework to meso- and microtidal wetlands, deltaic plains, and estuaries with contrasting sediment and water supplies will be essential for refining global coastal carbon budgets. This will help assess how tidal energy, sea-level rise, storms, and anthropogenic management shape the persistence and sequestration potential of buried carbon in diverse coastal landscapes.

6. Conclusions

This study provided new insights into OC dynamics across mudflats and salt-marshes of Aiguillon Bay (southwestern France). Variations in OC content and molecular composition (lignin and fatty acids) reflected the distinct biogeochemical environments shaped by both autochthonous production and lateral allochthonous inputs. Salt-marsh sediments emerged as a major contributor to carbon storage, due to their high OC content and mixed source signature, dominated by coastal marine POC and secondary halophytic vegetation inputs. Mudflat sediments were primarily influenced by marine inputs, with minor contributions (c. 9%) from microphytobenthos, which may have increased OM lability. Despite relatively similar sediment accumulation rates (1.8 vs. 2.2 cm yr^{-1}, respectively), the surface layers of the mudflat showed intense degradation, with a first-order decay rate approximately three times higher than in the salt-marsh (0.53 vs. 0.17 yr^{-1}). Nonetheless, the mudflat still supported substantial OC preservation at greater depths, meaningfully contributing to carbon burial at the decadal scale.

Organic matter preservation was closely tied to its molecular origin and sediment depth. Below habitat-specific active degradation zones —approximately 5 cm in the salt-marsh and 10 cm in the mudflat— the OM composition changed minimally, indicating reduced microbial transformation. Structurally resistant compounds persisted with depth through high lignin content, supporting important long-term carbon accumulation (366 gC m^{-2} yr^{-1} in salt-marsh, and 239 gC m^{-2} yr^{-1} in mudflats). The consistency of isotopic and biomarker signatures across depth indicated that net export of marsh-derived organic matter to adjacent mudflats is limited, suggesting limited outwelling under macrotidal conditions.

Altogether, these findings demonstrate the importance of using multiple biomarkers, and depth-resolved habitat-specific approaches for coastal carbon accounting. They also call for greater recognition of non-vegetated systems like mudflats, which can play a critical –yet often overlooked– role in coastal carbon budgets and long-term sedimentary carbon storage. By focusing on a macrotidal system with limited fluvial input, this study contributes to a broader understanding of carbon cycling in coastal wetlands and emphasizes the value of inclusive, habitat-spanning frameworks for carbon balance assessments.

CRediT authorship contribution statement

Amann Benjamin: Writing – review & editing, Writing – original draft, Visualization, Validation, Investigation, Formal analysis, Data curation. **Dubillot Bénédicte:** Writing – review & editing, Writing – original draft, Visualization, Validation, Methodology, Investigation, Formal analysis, Data curation, Conceptualization. **Eric Chaumillon:** Writing – review & editing, Validation, Investigation. **Cornelia Rumpel:** Writing – review & editing, Validation, Methodology, Data curation. **Marie-France Dignac:** Writing – review & editing, Validation, Methodology, Data curation. **Axel Felbacq:** Writing – review & editing, Validation, Methodology, Formal analysis, Data curation. **Sabine Schmidt:** Writing – review & editing, Validation, Methodology, Formal analysis, Data curation. **Maël Destampes:** Methodology, Formal analysis, Data curation. **Marie Arnaud:** Writing – review & editing, Validation, Methodology. **Edouard Metzger:** Writing – review & editing, Validation, Investigation. **Thomas Lacoue-Labarthe:** Writing – review & editing, Project administration, Funding acquisition, Conceptualization. **Christine Dupuy:** Writing – review & editing, Writing – original draft, Validation, Supervision, Project administration, Investigation, Funding acquisition, Data curation, Conceptualization.

Declaration of competing interest

The authors declare that they have no known competing financial interests or personal relationships that could have appeared to influence the work reported in this paper.

Acknowledgments

This work was supported by the project *La Rochelle Territoire Zero Carbone* (PIA TIGA #25875420; Caisse des Dépôts, Région Nouvelle-Aquitaine), as well as the *CarboNium* (ANR-22-PEXF-0006) and *CABESTAN* (ANR-22-PEXF-0007) projects that are both framed by the Priority Research Programmes and Equipments (PEPR) "FairCarboN", label France 2030 initiative. We thank all the laboratory platforms involved in this research: the IRMS platform (LIENSs Laboratory, La Rochelle), and the BGCI platform (IEES, PARIS). Special thanks go to Jean-Pierre Guéret (LPO, Conservator), Régis Gallais (OFB, Conservator) and their team at the réserve naturelle nationale de la baie de l'Aiguillon for their very close collaboration. We also thank all colleagues for their occasional help with field sampling.

Appendix A. Supplementary data

Supplementary data to this article can be found online at https://doi.org/10.1016/j.scitotenv.2026.181542.

Data availability

Data will be made available on request.

References

Aller, R.C., Cochran, J.K., 2019. The critical role of bioturbation for particle dynamics, priming potential, and organic C remineralization in marine sediments: local and basin scales. Front. Earth Sci. 7. https://doi.org/10.3389/feart.2019.00157.

Alongi, D.M., 2020. Carbon balance in salt marsh and mangrove ecosystems: a global synthesis. J. Mar. Sci. Eng. 8, 767. https://doi.org/10.3390/jmse8100767.

Amann, B., Chaumillon, E., Schmidt, S., Olivier, L., Jupin, J., Perello, M.C., Walsh, J.P., 2023. Multi-annual and multi-decadal evolution of sediment accretion in a saltmarsh of the French Atlantic coast: implications for carbon sequestration. Estuar. Coast. Shelf Sci. 293, 108467. https://doi.org/10.1016/j.ecss.2023.108467.

Amann, B., Eric, C., Xavier, B., Cécilia, P.-M., Perello, M.-C., Dupuy, C., Nathalie, L., Sabine, S., 2024. Understanding sediment and carbon accumulation in macrotidal minerogenic saltmarshes for climate resilience. Geomorphology 467, 109465. https://doi.org/10.1016/j.geomorph.2024.109465.

Arnaud, M., Bakhos, M., Rumpel, C., Dignac, M.-F., Bottinelli, N., Norby, R.J., Geairon, P., Deborde, J., Kostyrka, P., Gernigon, J., Lemesle, J.-C., Polsenaere, P., 2024. Salt marsh litter decomposition varies more by litter type than by extent of sea-level inundation. Commun. Earth Environ. 5, 686. https://doi.org/10.1038/s43247-024-01855-0.

Bassoullet, P., Le Hir, P., Gouleau, D., Robert, S., 2000. Sediment transport over an intertidal mudflat: field investigations and estimation of fluxes within the "Baie de Marennes-Oleron" (France). Cont. Shelf Res. 20, 1635–1653.

Baumann, J., Chaumillon, E., Schneider, J.-L., Jorissen, F., Sauriau, P.-G., Richard, P., Bonnin, J., Schmidt, S., 2017. Contrasting sediment records of marine submersion events related to wave exposure, Southwest France. Sediment. Geol. 353, 158–170. https://doi.org/10.1016/j.sedgeo.2017.03.009.

Berner, R.A., 1980. Early Diagenesis: A Theoretical Approach. Princeton University Press, p. 256 (ISBN: 9780691082608).

Bianchi, T.S., Canuel, E.A., 2011. Chemical Biomarkers in Aquatic Ecosystems, 2011. Princeton University Press, Princeton. https://doi.org/10.1515/9781400839100.

Bianchi, T.S., DiMarco, S.F., Smith, R.W., Schreiner, K.M., 2009. A gradient of dissolved organic carbon and lignin from Terrebonne–Timbalier Bay estuary to the Louisiana shelf (USA). Mar. Chem. 117, 32–41. https://doi.org/10.1016/j.marchem.2009.07.010.

Blanchard, G.F., Simon-Bouhet, B., Guarini, J.-M., 2002. Properties of the dynamics of intertidal microphytobenthic biomass. J. Mar. Biol. Assoc. U. K. 82, 1027–1028. https://doi.org/10.1017/S0025315402006574.

Bouillon, S., Boschker, H.T.S., 2006. Bacterial carbon sources in coastal sediments: a cross-system analysis based on stable isotope data of biomarkers. Biogeosciences 3, 175–185. https://doi.org/10.5194/bg-3-175-2006.

Bradley, J.A., Hülse, D., LaRowe, D.E., Arndt, S., 2022. Transfer efficiency of organic carbon in marine sediments. Nat. Commun. 13, 7297. https://doi.org/10.1038/s41467-022-35112-9.

Chaumillon, E., Tessier, B., Weber, N., Tesson, M., Bertin, X., 2004. Buried sandbodies within present-day estuaries (Atlantic coast of France) revealed by very high resolution seismic surveys. Mar. Geol. 211, 189–214. https://doi.org/10.1016/j.margeo.2004.07.004.

Chen, Z.L., Lee, S.Y., 2022. Tidal flats as a significant carbon reservoir in global coastal ecosystems. Front. Mar. Sci. 9, 900896. https://doi.org/10.3389/fmars.2022.900896.

Childers, D.L., Day, J.W., Mckellar, H.N., 2002. Twenty more years of marsh and estuarine flux studies: revisiting Nixon (1980). In: Weinstein, M.P., Kreeger, D.A. (Eds.), Concepts and Controversies in Tidal Marsh Ecology. Springer Netherlands, Dordrecht, pp. 391–423. https://doi.org/10.1007/0-306-47534-0_18.

Dai, J., Sun, M.-Y., Culp, R.A., Noakes, J.E., 2009. A laboratory study on biochemical degradation and microbial utilization of organic matter comprising a marine diatom, land grass, and salt marsh plant in estuarine ecosystems. Aquat. Ecol. 43, 825–841. https://doi.org/10.1007/s10452-008-9211-x.

Delaune, R.D., Patrick, W.H., Buresh, R.J., 1978. Sedimentation rates determined by 137Cs dating in a rapidly accreting salt marsh. Nature 275, 532–533. https://doi.org/10.1038/275532a0.

Dodet, G., Bertin, X., Bouchette, F., Gravelle, M., Testut, L., Wöppelmann, G., 2019. Characterization of sea-level variations along the metropolitan coasts of France: waves, tides, storm surges and long-term changes. J. Coast. Res. 88, 10. https://doi.org/10.2112/SI88-003.1.

Dodla, S.K., Wang, J.J., Cook, R.L., 2012. Molecular composition of humic acids from coastal wetland soils along a salinity gradient. Soil Sci. Soc. Am. J. 76, 1592–1605. https://doi.org/10.2136/sssaj2011.0346.

Douglas, T.J., Coops, N.C., Drever, M.C., Hunt, B.P.V., Martin, T.G., 2024. Linking microphytobenthos distribution and mudflat geomorphology under varying sedimentary regimes using unoccupied aerial vehicle (UAV)-acquired multispectral reflectance and photogrammetry. Sci. Total Environ. 942, 173675. https://doi.org/10.1016/j.scitotenv.2024.173675.

Goñi, M.A., Hedges, J.I., 1992. Lignin dimers: structures, distribution, and potential geochemical applications. Geochim. Cosmochim. Acta 56, 4025–4043. https://doi.org/10.1016/0016-7037(92)90014-A.

Goñi, M.A., Nelson, B., Blanchette, R.A., Hedges, J.I., 1993. Fungal degradation of wood lignins: geochemical perspectives from CuO-derived phenolic dimers and monomers. Geochim. Cosmochim. Acta 57, 3985–4002. https://doi.org/10.1016/0016-7037(93)90348-Z.

Goñi, M.A., Ruttenberg, K.C., Eglinton, T.I., 1998. A reassessment of the sources and importance of land-derived organic matter in surface sediments from the Gulf of Mexico. Geochim. Cosmochim. Acta 62, 3055–3075. https://doi.org/10.1016/S0016-7037(98)00217-8.

Goñi, M.A., Teixeira, M.J., Perkey, D.W., 2003. Sources and distribution of organic matter in a river-dominated estuary (Winyah Bay, SC, USA). Estuar. Coast. Shelf Sci. 57, 1023–1048. https://doi.org/10.1016/S0272-7714(03)00008-8.

Hedges, J.I., Ertel, J.R., 1982. Characterization of lignin by gas capillary chromatography of cupric oxide oxidation products. Anal. Chem. 54, 174–178. https://doi.org/10.1021/ac00239a007.

Hollander, M., Wolfe, D.A., Chicken, E., 2013. Nonparametric Statistical Methods, Third edition. John Wiley & Sons, New York, p. 848 (ISBN: 978-0-470-38737-5).

James, K., Macreadie, P.I., Burdett, H.L., Davies, I., Kamenos, N.A., 2024. It's time to broaden what we consider a 'blue carbon ecosystem'. Glob. Chang. Biol. 30, e17261. https://doi.org/10.1111/gcb.17261.

Kögel, I., Bochter, R., 1985. Characterization of lignin in forest humus layers by high-performance liquid chromatography of cupric oxide oxidation products. Soil Biol. Biochem. 17, 637–640. https://doi.org/10.1016/0038-0717(85)90040-9.

Ladd, C.J.T., Duggan-Edwards, M.F., Bouma, T.J., Pagès, J.F., Skov, M.W., 2019. Sediment supply explains long-term and large-scale patterns in salt marsh lateral expansion and erosion. Geophys. Res. Lett. 46, 11178–11187. https://doi.org/10.1029/2019GL083315.

Lamb, A.L., Wilson, G.P., Leng, M.J., 2006. A review of coastal palaeoclimate and relative sea-level reconstructions using δ13C and C/N ratios in organic material. Earth Sci. Rev. 75, 29–57. https://doi.org/10.1016/j.earscirev.2005.10.003.

Leorri, E., Zimmerman, A.R., Mitra, S., Christian, R.R., Fatela, F., Mallinson, D.J., 2018. Refractory organic matter in coastal salt marshes-effect on C sequestration calculations. Sci. Total Environ. 633, 391–398. https://doi.org/10.1016/j.scitotenv.2018.03.120.

Li, C., Cano, A., Acosta-Martinez, V., Veum, K.S., Moore-Kucera, J., 2020. A comparison between fatty acid methyl ester profiling methods (PLFA and EL-FAME) as soil health indicators. Soil Sci. Soc. Am. J. 84, 1153–1169. https://doi.org/10.1002/saj2.20118.

Liang, S., Li, H., Wu, H., Yan, B., Song, A., 2023. Microorganisms in coastal wetland sediments: a review on microbial community structure, functional gene, and environmental potential. Front. Microbiol. 14, 1163896. https://doi.org/10.3389/fmicb.2023.1163896.

Lin, T.-W., Tesi, T., Hefter, J., Grotheer, H., Wollenburg, J., Adolphi, F., Bauch, H., Nogarotto, A., Müller, J., Mollenhauer, G., 2025. Environmental controls of rapid terrestrial organic matter mobilization to the western Laptev Sea since the last deglaciation. Clim. Past 21, 753–772. https://doi.org/10.5194/cp-21-753-2025.

Macreadie, P.I., Akhand, A., Trevathan-Tackett, S.M., Duarte, C.M., Baldock, J., Bowen, J.L., Connolly, R.M., 2025. Stabilisation and destabilisation of coastal blue carbon: the key factors. Earth Sci. Rev. 265, 105133. https://doi.org/10.1016/j.earscirev.2025.105133.

Meziane, T., Bodineau, L., Retiere, C., Thoumelin, G., 1997. The use of lipid markers to define sources of organic matter in sediment and food web of the intertidal salt-marsh-flat ecosystem of Mont-Saint-Michel Bay, France. J. Sea Res. 38, 47–58. https://doi.org/10.1016/S1385-1101(97)00035-X.

Middelburg, J.J., 1989. A simple rate model for organic matter decomposition in marine sediments. Geochim. Cosmochim. Acta 53, 1577–1581. https://doi.org/10.1016/0016-7037(89)90239-1.

Middelburg, J.J., Herman, P.M.J., 2007. Organic matter processing in tidal estuaries. Mar. Chem. 106, 127–147. https://doi.org/10.1016/j.marchem.2006.02.007.

Moncelon, R., Metzger, E., Pineau, P., Emery, C., Bénéteau, E., De Lignières, C., Philippine, O., Robin, F.-X., Dupuy, C., 2022. Drivers for primary producers' dynamics: new insights on annual benthos pelagos monitoring in anthropised

freshwater marshes (Charente-Maritime, France). Water Res. 221, 118718. https://doi.org/10.1016/j.watres.2022.118718.
Ni, X., Zhao, G., White, J.R., Yao, P., Xu, K., Sapkota, Y., Liu, J., Zheng, H., Su, D., He, L., Liu, Q., Yang, S., Yuan, H., Ding, X., Zhang, Y., Ye, S., 2025. Source and degradation of soil organic matter in different vegetations along a salinity gradient in the Yellow River Delta wetland. CATENA 248, 108603. https://doi.org/10.1016/j.catena.2024.108603.
Odum, E.P., 1980. The status of three ecosystem-level hypotheses regarding salt marsh estuaries: tidal subsidy, outwelling, and detritus-based food chains. In: Estuarine Perspectives. Elsevier, pp. 485–495. https://doi.org/10.1016/B978-0-12-404060-1.50045-9.
Opsahl, S., Benner, R., 1995. Early Diagenesis of Vascular Plant Tissues: Lignin and Cutin Decomposition and Biogeochemical Implications, 59, pp. 4889–4904. https://doi.org/10.1016/0016-7037(95)00348-7.
Ouyang, X., Lee, S.Y., 2014. Updated estimates of carbon accumulation rates in coastal marsh sediments. Biogeosciences 11, 5057–5071. https://doi.org/10.5194/bg-11-5057-2014.
Qiao, Y., Liu, J., Zhao, M., Zhang, X.-H., 2018. Sediment depth-dependent spatial variations of bacterial communities in mud deposits of the Eastern China marginal seas. Front. Microbiol. 9, 1128. https://doi.org/10.3389/fmicb.2018.01128.
Regnier, P., Resplandy, L., Najjar, R.G., Ciais, P., 2022. The land-to-ocean loops of the global carbon cycle. Nature 603, 401–410. https://doi.org/10.1038/s41586-021-04339-9.
Santos, I.R., Burdige, D.J., Jennerjahn, T.C., Bouillon, S., Cabral, A., Serrano, O., Wernberg, T., Filbee-Dexter, K., Guimond, J.A., Tamborski, J.J., 2021. The renaissance of Odum's outwelling hypothesis in "Blue Carbon" science. Estuar. Coast. Shelf Sci. 255, 107361. https://doi.org/10.1016/j.ecss.2021.107361.
Savelli, R., Bertin, X., Orvain, F., Gernez, P., Dale, A., Coulombier, T., Pineau, P., Lachaussée, N., Polsenaere, P., Dupuy, C., Le Fouest, V., 2019. Impact of chronic and massive resuspension mechanisms on the microphytobenthos dynamics in a temperate intertidal mudflat. J. Geophys. Res. Biogeosci. 124, 3752–3777. https://doi.org/10.1029/2019JG005369.
Savoye, N., David, V., Morisseau, F., Etcheber, H., Abril, G., Billy, I., Charlier, K., Oggian, G., Derriennic, H., Sautour, B., 2012. Origin and composition of particulate organic matter in a macrotidal turbid estuary: The Gironde Estuary, France. Estuar. Coast. Shelf Sci. 108, 16–28. https://doi.org/10.1016/j.ecss.2011.12.005.
Schmidt, S., Amann, B., 2024. Depth profiles of selected radionuclides in marine sediments of three macrotidal saltmarshes of the French Atlantic coast. SEANOE. https://doi.org/10.17882/102639.
Stolpovsky, K., Dale, A.W., Wallmann, K., 2018. A new look at the multi-G model for organic carbon degradation in surface marine sediments for coupled benthic–pelagic simulations of the global ocean. Biogeosciences 15, 3391–3407. https://doi.org/10.5194/bg-15-3391-2018.
Teal, L., Bulling, M., Parker, E., Solan, M., 2008. Global patterns of bioturbation intensity and mixed depth of marine soft sediments. Aquat. Biol. 2, 207–218. https://doi.org/10.3354/ab00052.
Van de Broek, M., Vandendriessche, C., Poppelmonde, D., Merckx, R., Temmerman, S., Govers, G., 2018. Long-term organic carbon sequestration in tidal marsh sediments is dominated by old-aged allochthonous inputs in a macrotidal estuary. Glob. Chang. Biol. 24, 2498–2512. https://doi.org/10.1111/gcb.14089.
Vaughn, D.R., Bianchi, T.S., Shields, M.R., Kenney, W.F., Osborne, T.Z., 2020. Increased organic carbon burial in Northern Florida mangrove-salt marsh transition zones. Glob. Biogeochem. Cycles 34, e2019GB006334. https://doi.org/10.1029/2019GB006334.
Wang, Z.A., Kroeger, K.D., Ganju, N.K., Gonneea, M.E., Chu, S.N., 2016. Intertidal salt marshes as an important source of inorganic carbon to the coastal ocean. Limnol. Oceanogr. 61, 1916–1931. https://doi.org/10.1002/lno.10347.
Wang, F., Sanders, C.J., Santos, I.R., Tang, J., Schuerch, M., Kirwan, M.L., Kopp, R.E., Zhu, K., Li, X., Yuan, J., Liu, W., Li, Z., 2021. Global blue carbon accumulation in tidal wetlands increases with climate change. Natl. Sci. Rev. 8, nwaa296. https://doi.org/10.1093/nsr/nwaa296.
Weber, N., Chaumillon, É., Tesson, M., 2004. Enregistrement de la dernière remontée du niveau marin dans l'architecture interne d'une vallée incisée: le pertuis Breton (Charente-Maritime). Comptes Rendus Géoscience 336, 1273–1282. https://doi.org/10.1016/j.crte.2004.07.007.
Windham-Myers, L., Crooks, S., Troxler, T.G., 2019. A Blue Carbon Primer: The State of Coastal Wetland carbon Science, Practice, and Policy. Taylor & Francis Group, LLC, Boca Raton, FL 33487-2742.
Xia, S., Song, Z., Li, Q., Guo, L., Yu, C., Singh, B.P., Fu, X., Chen, C., Wang, Y., Wang, H., 2021. Distribution, sources, and decomposition of soil organic matter along a salinity gradient in estuarine wetlands characterized by C:N ratio, δ13C-δ15N, and lignin biomarker. Glob. Chang. Biol. 27, 417–434. https://doi.org/10.1111/gcb.15403.